Low Temperature Physics/Fizika Nizkikh Temperatur, 2012, v. 38, No. 8, pp. 905–911

Photodissociation and photochemistry of $V^+(H_2O)_n$, n = 1–4, in the 360–680 nm region

Björn Scharfschwerdt, Christian van der Linde, O. Petru Balaj, Ina Herber, Doreen Schütze, and Martin K. Beyer

Institut für Physikalische Chemie, Christian-Albrechts-Universität zu Kiel
Olshausenstraße 40, Kiel 24098, Germany
Email: beyer@phc.uni-kiel.de

Received April 25, 2012

The photodissociation and photochemistry of $V^+(H_2O)_n$, n = 1–4, was studied in the 360–680 nm region in a Fourier transform ion cyclotron resonance mass spectrometer. The light of a high pressure mercury arc lamp was filtered with band pass filters, with center wavelengths from 360 to 680 nm in steps of 20 nm. The bandwidth of the filters, defined as full width at half maximum, was 10 nm. Photodissociation channels are loss of water molecules, as well as loss of atomic or molecular hydrogen, which may be accompanied by loss of water molecules. The most intense absorptions are red shifted with increasing hydration. Theoretical spectra are calculated with time dependent density functional theory. Calculations reproduce all features of the experimental spectra, including the red shift with increasing hydration shell and the overall pattern of strong and weak absorptions.

PACS: **36.40.–c** Atomic and molecular clusters;
36.40.Mr Spectroscopy and geometrical structure of clusters;
36.40.Qv Stability and fragmentation of clusters.

Keywords: photochemistry, water activation, hydrogen formation, hydrated metal ion, electronic excitation.

Introduction

Hydrated singly-charged metal ions $M^+(H_2O)_n$ in the gas phase are interesting model systems for reactions of transient species in aqueous media [1]. Their properties have been investigated in considerable detail, with a wide range of experimental techniques, as reviewed recently [2–7]. Photodissociation in the O–H stretch region of the infrared, often coupled with tagging with a weakly bound species like Ar, is the most widely used spectroscopic method [8–14]. $V^+(H_2O)Ar$ [8] and $V^{2+}(H_2O)Ar_n$ [15] were characterized with infrared spectroscopy by Duncan and coworkers. For $V^+(H_2O)_n$, $n \leq 8$, a square-planar configuration was observed by Ohashi and coworkers, with four water molecules directly coordinated to V^+ [13]. Three H_2O were found to be coordinated to V^+ in a *T*-shaped arrangement [13].

Photodissociation of hydrated monovalent transition metal ions with electronic excitation of the metal center leads to loss of water [16–20], which is accompanied by water activation and loss of atomic hydrogen for $Fe^+(H_2O)_n$, $n \leq 10$ [16]. For $V^+(H_2O)$, the most intense absorption for the photodissociation $V^+(H_2O) \rightarrow V^+ + H_2O$ was observed at 629.7 nm [20]. For neutral V, spontaneous insertion of the metal into the O–H bond to form HVOH was observed in matrix isolation infrared spectra by Zhou *et al.* [21]. Broad-band photolysis with a high-pressure mercury arc lamp yields the bare oxide VO [21]. The potential energy surfaces of water activation by first-row transition metal ions were calculated in a series of papers by Ugalde and coworkers [22–26], showing that the case of Fe^+ is a typical example of two-state-reactivity [27]. For V^+, elimination of H_2 involves a curve crossing from the quintet to the triplet surface [24]. According to the calculated energies, the adiabatic threshold for H_2O elimination from $V^+(H_2O)$ lies at 1.663 eV, while the highest barrier along the reaction path to form $VO^+ + H_2$ lies significantly higher, 2.231 eV above $V^+(H_2O)$. For the current work, this means that H_2O loss is energetically accessible below 746 nm, while H_2 elimination is energetically allowed below 556 nm.

Armentrout and coworkers measured the water binding energies $M^+(H_2O)_n$, n = 1–4, for first-row transition metal ions Ti^+ through Cu^+ [28], and in all cases report that the structure of the studied species is a central metal ion with up to four solvating intact water molecules. For vanadium,

black-body radiation induced dissociation studies of larger clusters showed that atomic and molecular hydrogen can be eliminated with low activation energies from $V^+(H_2O)_n$, with n = 9–12 for atomic and n = 9–23 for molecular hydrogen [29].

To learn more about the electronic states and water activation pathways of hydrated monovalent vanadium ions, we investigated the photodissociation and photochemistry of $V^+(H_2O)_n$, n = 1–4, in the 360–680 nm region. Williams and coworkers routinely perform infrared spectroscopy of large ionic water clusters in a Fourier transform ion cyclotron resonance (FT-ICR) mass spectrometer, employing a cooled cell [30–33] and an infrared OPO [34]. Freiser and coworkers have shown that high-power lamps together with a monochromator or bandpass filters are ideally suited to conduct photodissociation experiments with transition metal complexes in an FT-ICR mass spectrometer [35–37]. Here, mass selected $V^+(H_2O)_n$, n = 1–4, which are trapped in an FT-ICR mass spectrometer at room temperature, are irradiated with the light of a high-pressure mercury arc lamp filtered by narrow bandpass filters. Experimental spectra are compared with theoretical spectra calculated by time-dependent density functional theory.

Experimental and computational details

The experiments are performed on a modified Bruker/Spectrospin CMS47X FT-ICR mass spectrometer, described in detail before [38–40]. Hydrated vanadium ions are produced by laser vaporization [41–43] of a solid vanadium disc, followed by supersonic expansion of the hot plasma in helium seeded with water vapor [29,39]. The ions are transferred with an electrostatic lens system to the ultra-high vacuum region of the mass spectrometer, where they are stored in the ICR cell at a pressure of typically $1\cdot10^{-10}$ mbar. After the supersonic expansion, the cluster ions have vibrational temperatures below 100 K. In the ICR cell, they are exposed to room temperature black-body radiation [44,45], gradually heating the clusters to a vibrational temperature around 300 K.

Light from a high-pressure mercury arc lamp (LEJ LQ-HXP 120-3) is guided with a liquid light guide to the rear end of the magnet, where it is collimated with a set of lenses and passed into the vacuum system through a glass viewport (Varian "Zero-Length", 7056 kodial glass). An internal wide-bandpass filter confines the lamp spectrum to 350–700 nm. To measure photodissociation spectra, external band-pass interference filters (Thorlabs) with a bandwidth of 10 nm full-width at half-maximum (FWHM) are used, covering center wavelengths from 360 to 680 nm in steps of 20 nm. The spectrum of the light was measured after the liquid light guide and the filters with a CCD-array spectrometer (*i*-trometer^{TM} 02, B&W Tek, Inc.) with a resolution of 2.5 nm. Figure 1 shows the spectrum of the lamp without (*a*) and with 10 nm bandwidth filters (*b*). The irradiation of the ions in the ICR cell is switched on and off with a fast internal shutter of the lamp, which is controlled from the APEX III data station of the ICR instrument. To determine the photon flux inside the ICR cell, the power was measured with a stabilized thermal power sensor (Thorlabs S302C).

Only those absorption events that lead to photodissociation are detected by our experiment, while fluorescence or phosphorescence are dark channels. The total photodissociation cross section σ is derived from the intensities of the reactant ion I_0 and the n product ions I_i, $i = 1 - n$, after irradiation for a time t with a photon flux Φ:

$$I_0 = \left(\sum_{i=0}^{n} I_i \right) \exp\left(-\sigma \Phi t\right). \qquad (1)$$

The photon flux was measured outside the ICR cell. Any change in alignment of the liquid light guide may have a substantial effect on the photon flux inside the ICR cell. As a consequence of the uncertainty in photon flux,

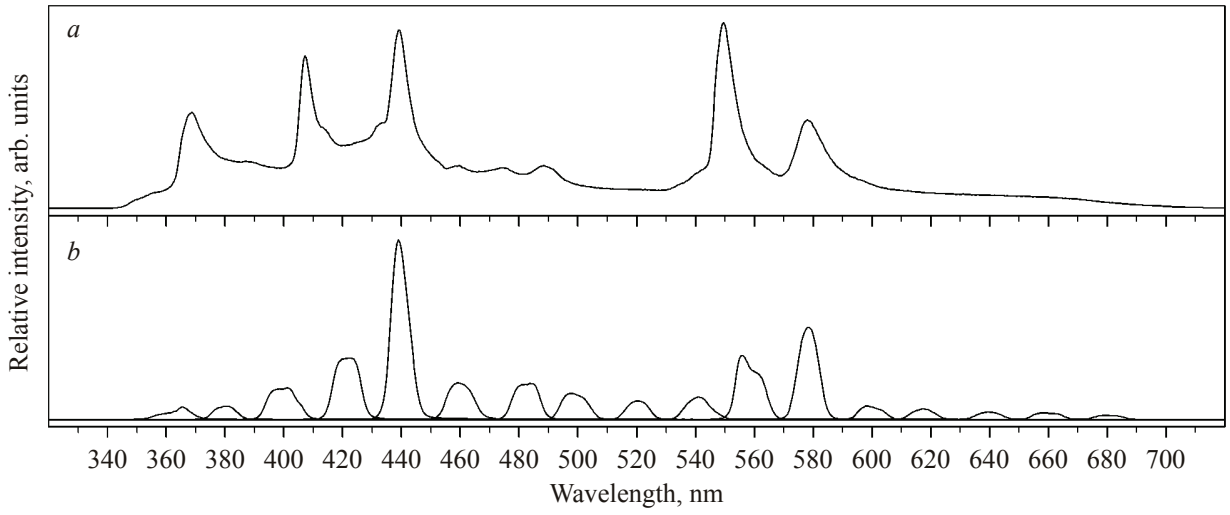

Fig. 1. White light emission spectrum of the high-pressure mercury arc lamp (*a*). Emission spectra of the lamp in combination with the 17 bandpass filters (*b*).

we estimate the uncertainty of relative as well as absolute total photodissociation cross sections to 30%. The contributions of the different photodissociation channels to the total cross section, however, are very reliable.

Electronic absorption spectra are calculated by time-dependent density functional theory with the B3LYP method and the 6-31+G(d) basis set for hydrogen and oxygen, and 6-311+G(2df) basis set for vanadium. The minimum structures reported by Ohashi and coworkers [13] were used as starting points for geometry optimizations. The local minimum character of the optimized structures was verified by frequency calculations. Electronic absorption spectra were calculated on the optimized geometries of the ground state as vertical excitation energies. All quantum chemical calculations were performed with Gaussian 09 [46].

Results

Three different experiments were performed for each cluster size $V^+(H_2O)_n$, n = 1–4. First, the mass selected ion was irradiated with the 350–700 nm "white" light of the lamp for different irradiation times, to learn whether the cluster undergoes any photochemical reaction at all. Second, the photodissociation spectrum of the mass selected cluster was measured with the 17 different available interference filters, with two to three different irradiation times. Third, at the wavelength with the highest photodissociation product yield, the kinetics of the photodissociation was investigated to check whether the observed photofragments are primary or secondary.

$V^+(H_2O)$. Figure 2 shows the mass spectra of the photodissociation experiment of $V^+(H_2O)$ with white light. After 15 s without irradiation, Fig. 2,*c*, the selected ion is still present, since it does not undergo black-body radiation induced dissociation. The fragments of larger clusters $V^+(H_2O)_n$, $n > 5$, which were not ejected because their intensities are below the noise level in the 0 s spectrum in (*a*), accumulate in the n = 4–6 ions due to black-body radiation induced dissociation. After 15 s irradiation with white light, Fig. 2,*d*, V^+ and VO^+ are observed as photofragments. Due to the incomplete mass selection, however, VO^+ may, at least in part, be the photofragment of larger clusters $n > 5$.

Interestingly, no photofragments were detected using the 10 nm bandpass filters. We attribute this puzzling behavior to unfavorable circumstances: The most intense absorption of $V^+(H_2O)$ at 629.7 nm [20] is not covered by our bandpass filters, and the overall light intensity in the strong absorption band of $V^+(H_2O)$ is low. The calculated absorption spectrum of $V^+(H_2O)$, shown in Fig. 3, supports this interpretation. The strong allowed transitions lie below 360 nm, while some weaker transitions emerge above 680 nm, outside the experimentally studied range.

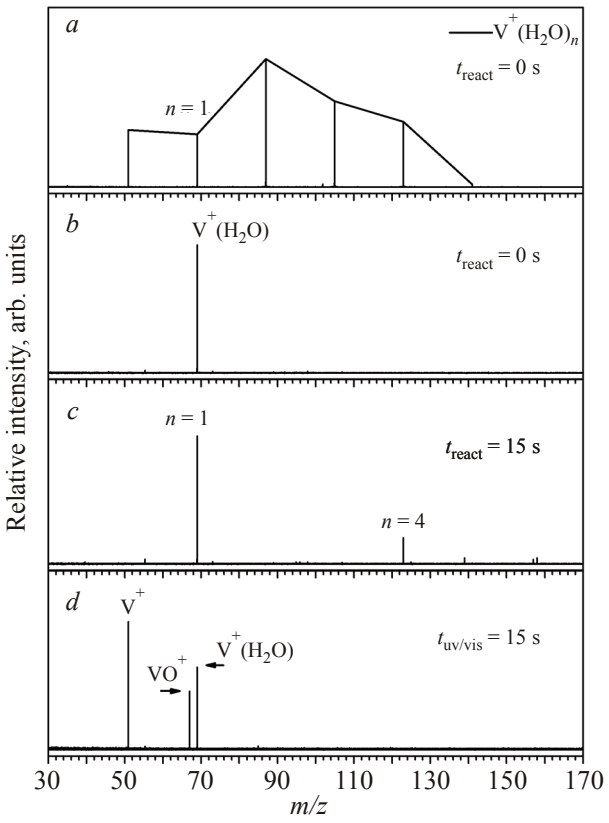

Fig. 2. Mass spectra of the photodissociation experiment of $V^+(H_2O)$ with white light. Mass spectrum before (*a*) and after mass selection (*b*). After 15 s without irradiation (*c*), the selected ion is still present, since it does not undergo black-body radiation induced dissociation. The fragments of larger clusters, which were not ejected because they are below the noise level in the 0 s spectrum in (*a*), accumulate in the n = 4–6 ions due to black-body radiation induced dissociation (*c*). After 15 s irradiation with white light, V^+ and VO^+ are observed as photofragments. Due to the incomplete mass selection, however, VO^+ may, at least in part, be a photofragment of larger clusters (*d*).

$V^+(H_2O)_2$. For the n = 2 cluster, V^+, $V^+(H_2O)$, VO^+ and $VO^+(H_2O)$ are confirmed photodissociation products after 15 s irradiation with white light. VOH^+ and $VOH^+(H_2O)$ are observed in traces. In this case, mass selection was complete, so that the interference from larger clusters discussed above does not occur for this cluster

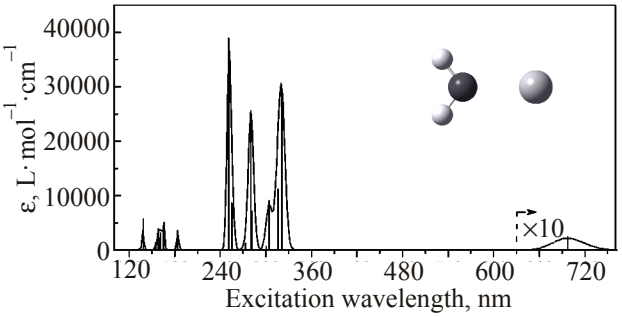

Fig. 3. Calculated absorption spectrum of $V^+(H_2O)$. The region above 630 nm is multiplied by 10 to display the weak absorption.

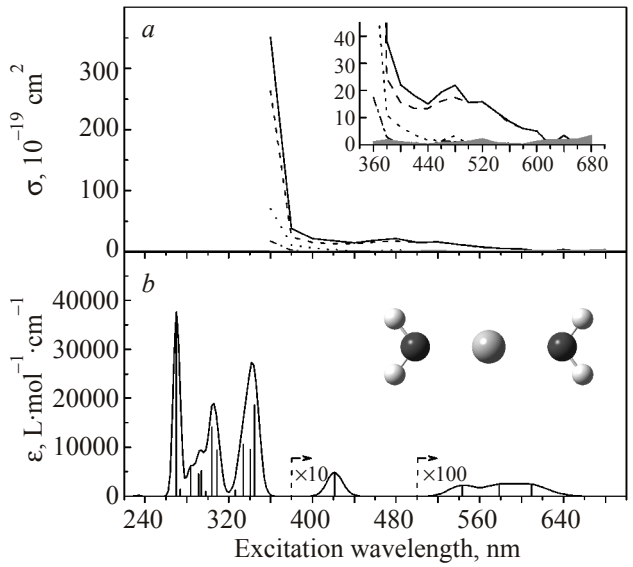

Fig. 4. Experimental (*a*) and calculated (*b*) spectrum of $V^+(H_2O)_2$. The experimental spectrum, measured with 15 s irradiation time, is split into contributions from the different photochemical reactions, i.e., loss of one or two H_2O (dashed line), loss of H_2 and zero or one H_2O (dotted line), and loss of H (dash-dotted line). The intensity of weak absorptions is multiplied as indicated in the figure.

size. The measured spectrum, shown in Fig. 4,*a*, exhibits the calculated features, Fig. 4,*b*. The most intense absorption is measured at 360 nm, at the blue end of the investigated spectral range, and it is conceivable that it is only the onset of an intense, broad peak in the UV. Weak absorptions are detected up to 640 nm, with a clear maximum at 480 nm, shifted by 60 nm from the calculated local absorption maximum at 420 nm. H and H_2 elimination contribute 5% and 20% to the spectral intensity at 360 nm, but their contribution vanishes below the noise level above 480 nm.

The photodissociation kinetics at 360 nm, Fig. 5, confirm that V^+, $V^+(H_2O)$ and VO^+ are primary photodissociation products. The kinetics, however, can only be fitted if an induction period is assumed, in which an unreactive fraction of $V^+(H_2O)_2$ is converted to a reactive one. We assume that the initially cold clusters, with vibrational temperatures from the supersonic expansion well below 100 K, show narrow absorption lines and therefore weak overlap with the irradiated broad-band light. After exposure to room temperature black-body radiation [44,45], the clusters reach vibrational temperatures around 300 K, and the absorptions broaden. As soon as the clusters are in thermal equilibrium with the environment, the kinetics is first-order. Since the conversion of the photofragment intensities to spectral absorption cross section assumes true first-order behavior, the absolute cross sections as well as the relative intensities in the optical spectra are not fully reliable.

$V^+(H_2O)_3$. The parent cluster $V^+(H_2O)_3$ is depleted after 4 s irradiation with white light. Loss of two and three

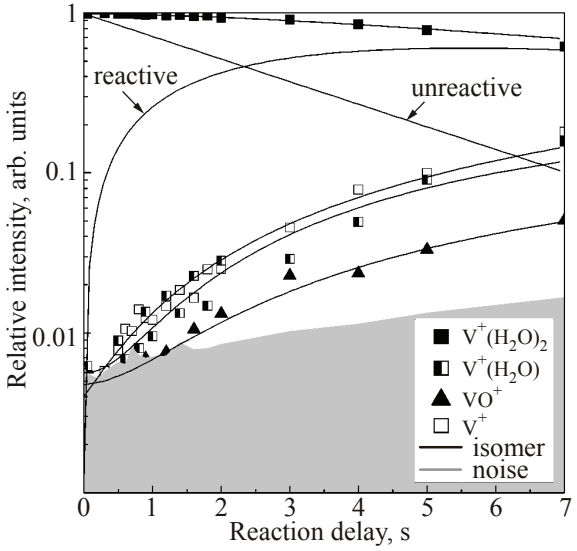

Fig. 5. Photodissociation kinetics of $V^+(H_2O)_2$, measured with the 360 nm bandpass filter. During an induction period, the initially unreactive fraction of $V^+(H_2O)_2$ is converted to a reactive one.

H_2O to form $V^+(H_2O)$ and V^+ dominates. H_2 elimination is also strong, accompanied by the loss of one or two H_2O to form $VO^+(H_2O)$ and VO^+, respectively. Only traces of $VOH^+(H_2O)$ and $VOH^+(H_2O)_2$ are observed, corresponding to the loss of H and one or zero H_2O, respectively. In the experimental spectrum, Fig. 6,*a*, the three different photochemical channels exhibit a strong maximum at 400 nm, with two weaker maxima at 520 and 620 nm. The calculated spectrum, Fig. 6,*b*, exhibits similar features, reproducing the relative intensities of strong and weak ab-

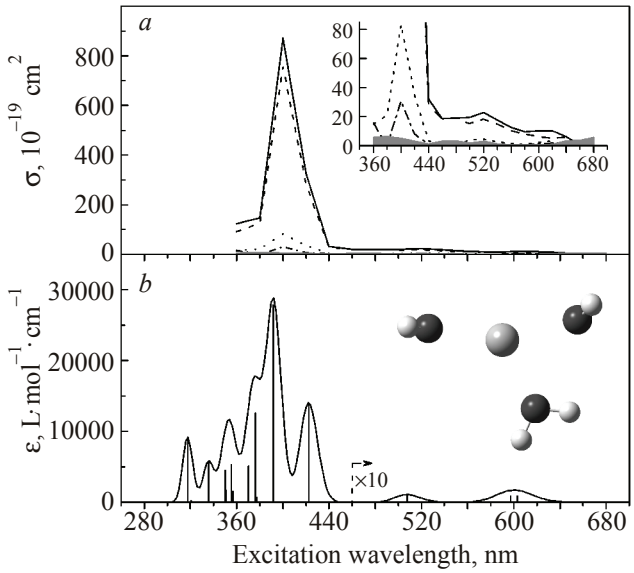

Fig. 6. Experimental (*a*) and calculated (*b*) spectrum of $V^+(H_2O)_3$. The experimental spectrum, measured with 4–15 s irradiation time, i.e., loss of one or two H_2O (dashed line), loss of H_2 and zero or one H_2O (dotted line), and loss of H and zero or one H_2O (dash-dotted line). The intensity of weak absorptions is multiplied as indicated in the figure.

sorptions very well. The experiment, with the 20 nm spacing of the filters, does not resolve the calculated peaks in the 360–440 nm region, but the intensity drop at 360–380 nm is in agreement with the calculation.

Fitting the photodissociation kinetics at 400 nm again requires an induction period, which is considerably shorter than for $n = 2$. This supports the interpretation that the induction period is caused by equilibration of the clusters with the room temperature black-body radiation environment. The kinetics again confirms the primary product character of the water and H_2 loss channels, while H elimination was too weak to be included into the kinetics.

$V^+(H_2O)_4$. With white light, photodissociation leads to loss of two to four water molecules from $V^+(H_2O)_4$ after 4 s irradiation. In contrast to the $n = 2$ and $n = 3$ cases, however, loss of a hydrogen atom is more abundant than loss of molecular H_2. Thermochemically, H_2 loss is favored over H loss, since it is accompanied by loss of one to three H_2O molecules, with a maximum at two H_2O, while H atom loss is accompanied by loss of zero to two H_2O, with a maximum at one H_2O. The experimental spectrum, shown in Fig. 7,*a*, reveals that H loss is more abundant than H_2 loss over the whole spectrum, but pure H_2O loss dominates at all wavelengths. The spectrum exhibits a pronounced maximum at 460 nm, with a second clear maximum at 400 nm. Towards the red end of the spectrum, the intensity drops sharply from the 460 nm maximum down to a plateau at 520 nm. Further intensity drops are observed at 580 and 620 nm. But even at 680 nm, the longest wavelength investigated, light-induced loss of H_2O is clearly detected. The calculated spectrum, Fig. 7,*b*, again reproduces the measured intensity pattern very well, but the transitions around 440 and 480 nm seem closer together in the experiment. With more densely spaced filters, the two peaks might be resolved.

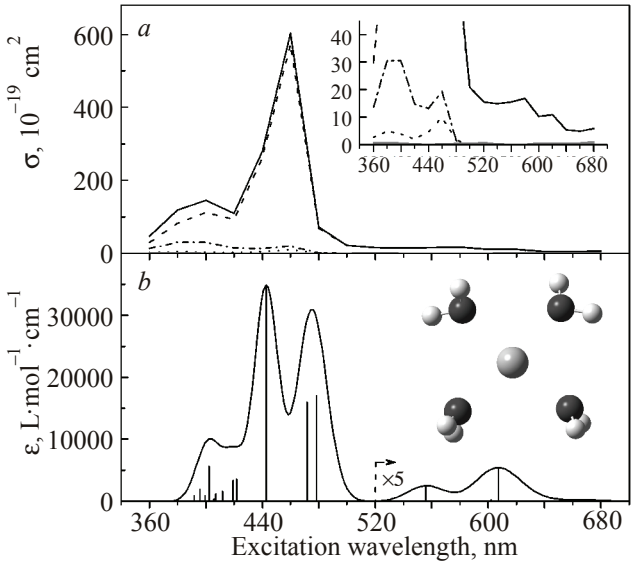

Fig. 7. Experimental (*a*) and calculated (*b*) spectrum of $V^+(H_2O)_4$. The experimental spectrum, measured with 4 s irradiation time, is split into contributions from the different photochemical reactions, i.e., loss of 1–4 H_2O (dashed line), loss of H_2 and 0–2 H_2O (dotted line), and loss of H and 0–2 H_2O (dash-dotted line). Only for $V^+(H_2O)_4$, H loss is more intense than H_2 loss. The intensity of weak absorptions is multiplied as indicated in the figure.

The photodissociation kinetics at 440 nm exhibits a very short induction period, in line with the thermalization argument. The kinetics confirms the primary product character of the water and H loss channels. Here the intensity of H_2 elimination products was too weak to be included in the kinetics.

Discussion

In the bare V^+ ion, the allowed $3d^3(^3F)4p \leftarrow 3d^4$ transitions lie around 270 nm [47]. Solvation with water progressively shifts these transitions to the red, with observed maxima below 360 nm, at 400 nm and at 460 nm for $n = 2$, 3 and 4, respectively. With the help of the calculations, we can extend this trend. The strong absorption with the longest wavelength shifts from 320 nm via 340 nm and 420 nm to 480 nm for $n = 1$–4, respectively. The weaker transitions at longer wavelengths are due to transitions corresponding to $3d^34s \leftarrow 3d^4$ and $3d^4 \leftarrow 3d^4$ transitions in V^+, which are parity forbidden in the atomic ion.

It is tempting to say that water activation with H or H_2 loss occurs only after excitation into a V^+ 4*p* orbital. The signal-to-noise ratio, however, at the weaker transitions is such that the contributions of these minor reaction channels may lie below the noise level. Very interesting is the undoubted fact that H elimination is dominant for $n = 4$. With activation by black-body radiation, H elimination was observed only in a very narrow size range of $V^+(H_2O)_n$, $n = 9$–12 [29]. It will be very interesting to study the photodissociation spectra for $n = 5$–12, because the spectral characteristics of the H elimination channel may eventually lead to an explanation of this intriguing behavior.

Conclusion and outlook

With a high-pressure mercury arc lamp and bandpass filters, it is possible to acquire photodissociation spectra of hydrated ions with a decent signal-to-noise ratio and a dynamic range of three orders of magnitude in an FT-ICR mass spectrometer. $V^+(H_2O)_n$, $n = 1$–4, show a characteristic photochemistry. The strongest absorption is derived from the $3d^3(^3F)4p \leftarrow 3d^4$ transition of the atomic ion. This transition is progressively red-shifted with increasing solvent shell. Theoretical spectra calculated with time-dependent density functional theory agree very well with experiment, and reproduce all the strong and weak absorption maxima, with deviations of 20 nm or less.

These first results are encouraging, but there is, of course, room for improvement. In future studies, a filter set

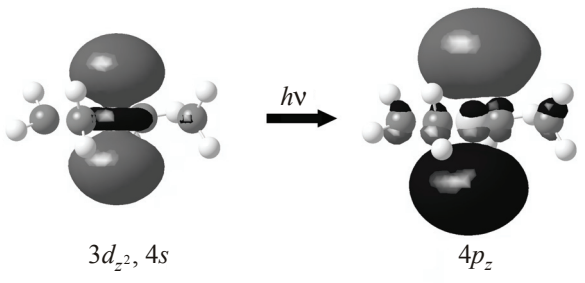

Fig. 8. Representative molecular orbitals (MOs) for a strong transition calculated at 442,84 nm in $V^+(H_2O)_4$. The ground-state MO is a linear combination of the vanadium $3d_{z^2}$ and 4*s* atomic orbitals. The excited state MO corresponds to the vanadium $4p_z$ orbital.

with a spacing of 10 nm should be used. A tungsten halogen lamp should be superior to the high-pressure mercury arc lamp, since its light has a smoother intensity distribution, reducing the risk of distortions of the spectra due to local intensity maxima of the lamp. For larger clusters, the rate of black-body radiation induced dissociation should be reduced by cooling the environment. Quantitative absorption cross sections are only reliable if the induction period is over before illumination starts, so that the photochemical reaction kinetics exhibits true first-order behavior.

Acknowledgements

Financial support from the Deutsche Forschungsgemeinschaft, grant no. BE2505/4-2, is gratefully acknowledged.

1. B.S. Fox, O.P. Balaj, I. Balteanu, M.K. Beyer, and V.E. Bondybey, *Chem. Eur. J.* **8**, 5534 (2002).
2. M.A. Duncan, *Annu. Rev. Phys. Chem.* **48**, 69 (1997).
3. M.A. Duncan, *Int. J. Mass Spectrom.* **200**, 545 (2000).
4. K. Fuke, K. Hashimoto, and S. Iwata, *Adv. Chem. Phys.* **110**, 431 (1999).
5. G. Niedner-Schatteburg and V.E. Bondybey, *Chem. Rev.* **100**, 4059 (2000).
6. V.E. Bondybey and M.K. Beyer, *Int. Rev. Phys. Chem.* **21**, 277 (2002).
7. M.K. Beyer, *Mass Spectrom. Rev.* **26**, 517 (2007).
8. V. Kasalova, W.D. Allen, H.F. Schaefer, E.D. Pillai, and M.A. Duncan, *J. Phys. Chem.* **A111**, 7599 (2007).
9. P.D. Carnegie, B. Bandyopadhyay, and M.A. Duncan, *J. Phys. Chem.* **A112**, 6237 (2008).
10. P.D. Carnegie, B. Bandyopadhyay, and M.A. Duncan, *J. Phys. Chem.* **A115**, 7602 (2011).
11. R.S. Walters, E.D. Pillai, and M.A. Duncan, *J. Am. Chem. Soc.* **127**, 16599 (2005).
12. T. Iino, K. Ohashi, K. Inoue, K. Judai, N. Nishi, and H. Sekiya, *J. Chem. Phys.* **126**,–(2007).
13. J. Sasaki, K. Ohashi, K. Inoue, T. Imamura, K. Judai, N. Nishi, and H. Sekiya, *Chem. Phys. Lett.* **474**, 36 (2009).
14. K. Furukawa, K. Ohashi, N. Koga, T. Imamura, K. Judai, N. Nishi, and H. Sekiya, *Chem. Phys. Lett.* **508**, 202 (2011).
15. B. Bandyopadhyay and M. Duncan, *Chem. Phys. Lett.* **530**, 10 (2012).
16. L. Dukan, L. del Fabbro, P. Pradel, O. Sublemontier, J.M. Mestdagh, and J.P. Visticot, *Eur. Phys. J.* **D3**, 257 (1998).
17. L. Poisson, L. Dukan, O. Sublemontier, F. Lepetit, F. Reau, P. Pradel, J.M. Mestdagh, and J.P. Visticot, *Int. J. Mass Spectrom.* **220**, 111 (2002).
18. L. Poisson, P. Pradel, F. Lepetit, F. Reau, J.M. Mestdagh, and J.P. Visticot, *Eur. Phys. J.* **D14**, 89 (2001).
19. J.S. Daluz, A. Kocak, and R.B. Metz, *J. Phys. Chem.* **A116**, 1344 (2012).
20. D.E. Lessen, R.L. Asher, and P.J. Brucat, *J. Chem. Phys.* **93**, 6102 (1990).
21. M. Zhou, J. Dong, L. Zhang, and Q. Qin, *J. Am. Chem. Soc.* **123**, 135 (2001).
22. A. Irigoras, J.E. Fowler, and J.M. Ugalde, *J. Phys. Chem.* **A102**, 293 (1998).
23. A. Irigoras, J.E. Fowler, and J.M. Ugalde, *J. Am. Chem. Soc.* **121**, 8549 (1999).
24. A. Irigoras, J.E. Fowler, and J.M. Ugalde, *J. Am. Chem. Soc.* **121**, 574 (1999).
25. A. Irigoras, O. Elizalde, I. Silanes, J.E. Fowler, and J.M. Ugalde, *J. Am. Chem. Soc.* **122**, 114 (2000).
26. S. Chiodo, O. Kondakova, M.D. Michelini, N. Russo, E. Sicilia, A. Irigoras, and J.M. Ugalde, *J. Phys. Chem.* **A108**, 1069 (2004).
27. D. Schröder, S. Shaik, and H. Schwarz, *Acc. Chem. Res.* **33**, 139 (2000).
28. N.F. Dalleska, K. Honma, L.S. Sunderlin, and P.B. Armentrout, *J. Am. Chem. Soc.* **116**, 3519 (1994).
29. B.S. Fox, I. Balteanu, O.P. Balaj, H.C. Liu, M.K. Beyer, and V.E. Bondybey, *Phys. Chem. Chem. Phys.* **4**, 2224 (2002).
30. X.H. Guo, M. Duursma, A. Al-Khalili, L.A. McDonnell, and R.M.A. Heeren, *Int. J. Mass Spectrom.* **231**, 37 (2004).
31. R.L. Wong, K. Paech, and E.R. Williams, *Int. J. Mass Spectrom.* **232**, 59 (2004).
32. O.P. Balaj, C.B. Berg, S.J. Reitmeier, V.E. Bondybey, and M.K. Beyer, *Int. J. Mass Spectrom.* **279**, 5 (2009).
33. O. Hampe, T. Karpuschkin, M. Vonderach, P. Weis, Y.M. Yu, L.B. Gan, W. Klopper, and M.M. Kappes, *Phys. Chem. Chem. Phys.* **13**, 9818 (2011).
34. M.F. Bush, R.J. Saykally, and E.R. Williams, *J. Am. Chem. Soc.* **130**, 15482 (2008).
35. C.J. Cassady and B.S. Freiser, *J. Am. Chem. Soc.* **106**, 6176 (1984).
36. R.L. Hettich, T.C. Jackson, E.M. Stanko, and B.S. Freiser, *J. Am. Chem. Soc.* **108**, 5086 (1986).
37. L.M. Roth and B.S. Freiser, *Mass Spectrom. Rev.* **10**, 303 (1991).
38. C. Berg, T. Schindler, G. Niedner-Schatteburg, and V.E. Bondybey, *J. Chem. Phys.* **102**, 4870 (1995).
39. M. Beyer, C. Berg, H.W. Görlitzer, T. Schindler, U. Achatz, G. Albert, G. Niedner-Schatteburg, and V.E. Bondybey, *J. Am. Chem. Soc.* **118**, 7386 (1996).
40. R.F. Höckendorf, O.P. Balaj, C. van der Linde, and M.K. Beyer, *Phys. Chem. Chem. Phys.* **12**, 3772 (2010).

41. V.E. Bondybey and J.H. English, *J. Chem. Phys.* **74**, 6978 (1981).
42. T.G. Dietz, M.A. Duncan, D.E. Powers, and R.E. Smalley, *J. Chem. Phys.* **74**, 6511 (1981).
43. S. Maruyama, L.R. Anderson, and R.E. Smalley, *Rev. Sci. Instrum.* **61**, 3686 (1990).
44. R.C. Dunbar, *Mass Spectrom. Rev.* **23**, 127 (2004).
45. B.S. Fox, M.K. Beyer, and V.E. Bondybey, *J. Phys. Chem.* **A105**, 6386 (2001).
46. M.J. Frisch, G.W. Trucks, H.B. Schlegel, G.E. Scuseria, M.A. Robb, J.R. Cheeseman, G. Scalmani, V. Barone, B. Mennucci, G.A. Petersson, *et al.*, *Gaussian 09, Revision B.01*, Gaussian, Inc., Wallingford CT (2010).
47. Y. Ralchenko, A.E. Kramida, J. Reader, and NIST ASD Team, *NIST Atomic Spectra Database (ver. 4.1.0)*, *http://physics.nist.gov/asd* (2012).